Journal of Electron Spectroscopy and Related Phenomena 266 (2023) 147364

Contents lists available at ScienceDirect

Journal of Electron Spectroscopy and Related Phenomena

journal homepage: www.elsevier.com/locate/elspec

Atomically dispersed Ni-N-C electrocatalysts, studied by Ni L-edge spectro-ptychography

Chunyang Zhang [a,b], Jiatang Chen [a], Hao Yuan [b,1], Jian Wang [c], Tianxiao Sun [c,d], Drew Higgins [a], Adam P. Hitchcock [b,*]

[a] Dept. of Chemical Engineering, McMaster University, Hamilton, ON L8S 4M1, Canada
[b] Dept. of Chemistry & Chemical Biology, McMaster University, Hamilton, ON L8S 4M1, Canada
[c] Canadian Light Source, Saskatoon SK S7N 2V, Canada
[d] Helmholtz Zentrum Berlin, BessyII, Hahn-Meitner-Platz 1, 14109 Berlin, Germany

ARTICLE INFO

Keywords:
Atomically dispersed Ni electrocatalysts
Spectro-ptychography
Scanning transmission X-ray microscopy
Defocused
Reduced dose

ABSTRACT

Soft X-ray spectro-ptychography of nickel-nitrogen-carbon electrocatalysts containing atomically dispersed Ni-based active sites were measured at the Ni L_3 edge. Samples prepared with two different loadings of Ni precursors were investigated and compared to the results of an earlier study using scanning transmission X-ray microscopy (STXM) [Zhang et al., ACS Catalysis 12 (2022) 8746]. The ptychography data sets were measured using a defocused probe (1–3 μm). The spatial resolution was improved from ~60 nm (STXM) to ~20 nm (ptychography). Spectro-ptychography stacks were measured at 4 component-specific energies (4-E stack) and at many energies across the full Ni L_3 edge (34-E stack). Maps of three key chemical components (Ni metal, Ni_3S_2, and atomically dispersed N-coordinated Ni catalyst sites) were derived by fits of suitable reference spectra to absorption signals derived from the amplitude images from ptychographic reconstruction. The spectro-ptychography 4-E and 34-E stacks gave chemical mapping similar to each other and to the earlier STXM results. The phase signals obtained from the same data set and reconstruction were also found to be analyzable using reference phase spectra extracted from the phase stack, which generated chemical maps similar to those based on ptychography amplitude data. By using a defocused probe, the radiation dose and acquisition times for spectro-ptychography are comparable to conventional STXM, but significantly improved spatial resolution was achieved. This study highlights the added value of spectro-ptychography relative to STXM for studies of electrocatalysts.

1. Introduction

Metal-nitrogen-carbon (M-N-C) nanostructures, commonly referred to as atomically dispersed M-N_x/C catalysts, are a promising class of materials for electrocatalytic applications.[1–4] In particular, nickel-nitrogen-carbon (Ni–N–C) atomically dispersed electrocatalysts have shown activity and high selectivity to generate CO through the electrochemical CO_2 reduction (CO_2R) reaction. [5,6] The catalytic activity of M-N-C materials has been attributed to well-dispersed single metal atoms in the form of nitrogen-coordinated (MN_x) active sites on highly conductive carbon materials. [7,8] Recently we reported a detailed, multi-edge (Ni 2p, S 2p, N 1 s, O 1 s, C 1 s) X-ray spectromicroscopy investigation of Ni-N-C catalysts using scanning transmission X-ray microscopy (STXM) [9], combined with measurements of catalysis performance and electron microscopic characterization. STXM provides a large-scale (tens of microns) overview of the catalyst morphology while achieving chemical mapping at ~50 nm spatial resolution. [10,11] This technique complements much higher spatial resolution methods, such as transmission electron microscopy (TEM) imaging [12] combined with atomic resolution electron energy loss spectroscopy (EELS) [6,13]; and non-spatially resolved methods, such as X-ray absorption spectroscopy (XAS). [14,15].

In our previous work [9] pyrolyzed, polymer-derived Ni-N-C catalysts were analyzed using STXM spectromicroscopy to determine the chemical states present and to quantitatively map their spatial distribution. From the Ni L_{23} near edge X-ray absorption (NEXAFS) spectra,

* Corresponding author.
E-mail address: aph@mcmaster.ca (A.P. Hitchcock).
[1] present address: University of Victoria, Victoria, BC

https://doi.org/10.1016/j.elspec.2023.147364
Received 28 April 2023; Received in revised form 21 June 2023; Accepted 22 June 2023
Available online 1 July 2023

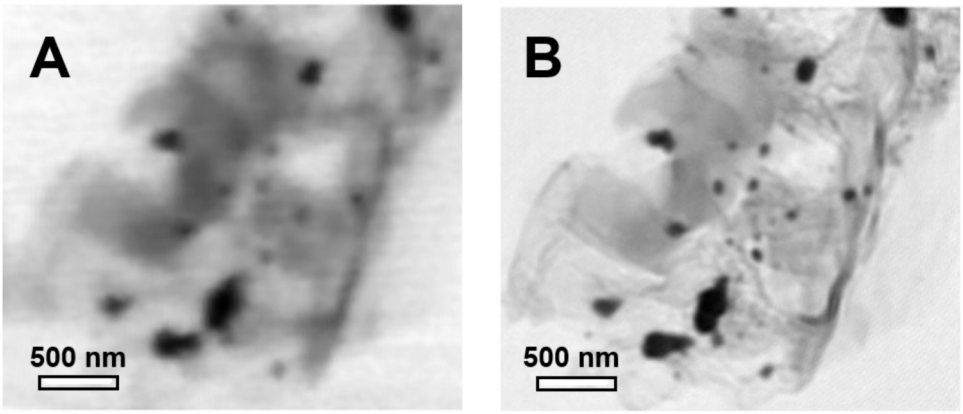

Fig. 1. Comparison of STXM and ptychography images. (a) STXM transmission image at 852.7 eV of the Ni-N-C-high sample [3 ms/pixel, (4 μm)^2 (156)^2 pixels, total acquisition time of 6 min]. (b) Ptychography amplitude image of the same area, at the same photon energy. The diffraction images were measured with a 1.25 μm defocus spot, 32 × 32 spots, with 90% overlap and 3.0 s dwell. Total acquisition time was 29 min.

metallic Ni (referred to as Ni metal in this work), as well as tri-nickel disulphide (Ni_3S_2) and atomically dispersed NiN_x/C species, which were approximated by 5,10,15,20-tetraphenyl- 21 H,23 H-porphine nickel (II) (NiTPP), were identified and mapped. [9] Although STXM spectromicroscopy is very powerful, the spatial resolution achieved with commonly available zone plate lenses is typically 40–60 nm. A significant improvement in spatial resolution can be achieved using ptychography. [16,17] While hard X-ray ptychography is well established, soft X-ray ptychography has only emerged recently. [18–25] Here we have used soft X-ray spectro-ptychography at the Ni L-edge to study the same Ni-N-C catalyst samples previously investigated by STXM, in order to explore the additional information that higher spatial resolution ptychography can provide. The measurements were performed using the ptychography capability recently developed at the ambient-STXM at the Canadian Light Source (CLS). [26–28] The single channel phosphor / photomultiplier detector was replaced by a direct X-ray detecting, charge-coupled device (CCD) camera, which allows imaging of the X-rays coherently scattered from the sample. High-resolution real-space images are generated from the measured coherent diffraction patterns through a ptychography reconstruction software package, PyPIE [26], which is based on the extended ptychographic iterative engine (ePIE) phase retrieval algorithm. [17] The spatial resolution of ptychography is not limited by the properties of focusing optics (indeed ptychography has been referred to as 'lens-less imaging'). It has the potential to reach the far-field optical resolution limit, which is 0.61 * λ/NA where λ is the X-ray wavelength and NA is the numerical aperture – thus of the order of 3 nm at the C K edge and 1 nm at the Ni L edge. Currently, the best spatial resolution achieved by soft X-ray ptychography is ~3 nm at 1500 eV. [18] In this work, a direct comparison of the ptychography and STXM results from the same area of a Ni-N-C catalyst showed a ~3-fold improvement in spatial resolution from ~60 to ~20 nm, while achieving similar chemical mapping. These results reinforce the conclusions previously reached regarding the links between the catalytic activity and morphology of these materials.

2. Experimental methods

2.1. Sample preparation

As described elsewhere [9,29], Ni-N-C catalysts with high-loading Ni content (Ni-N-C-high) and low-loading Ni content (Ni-N-C-low) were synthesized by heat-treating a mixture of aniline (1 mL, Sigma-Aldrich), cyanamide (2 g, Sigma-Aldrich) and different amounts of nickel chloride hexahydrate ($NiCl_2 \cdot 6\ H_2O$,Sigma-Aldrich) [Ni-N-C-high (1.2 g) and Ni-N-C-low (0.08 g)] in a 1.5 M HCl solution (200 mL, ACS reagent). After thorough mixing, ammonium persulfate (1.5 g, Sigma-Aldrich) was added as an oxidant to polymerize the aniline to polyaniline. The resulting product was pyrolyzed at 900 °C in argon for 1 hr followed by an acid washing process to remove surface-exposed labile Ni compounds. A second pyrolysis at 900 °C in argon for 3 hrs was then performed. Reference compounds for spectroscopy analysis included physical vapor deposition Ni metal, 5,10,15,20-tetraphenyl- 21 H,23 H-porphine nickel (II) (NiTPP) (Sigma-Aldrich) and Ni_3S_2 (Sigma-Aldrich).

2.2. STXM measurements and analysis

The catalytic powders were physically deposited in the dry state onto formvar coated 3 mm Cu grids. Poorly adhering particles and large agglomerates were removed by tapping the grid on a hard surface. STXM and spectro-ptychographic imaging were performed at the soft X-ray spectromicroscopy beamline (SM) 10ID-1 at the Canadian Light Source (CLS, Saskatoon, Canada). [30] Spectroscopic information was obtained by recording raster scanned image sequences (also known as stacks [31]). The energy scale of the beamline was calibrated by recording the spectrum of neon gas. [32] STXM images, point spectra, and stacks were analyzed using aXis2000. [33,34] Stacks were first aligned using Fourier cross-correlation procedures, then converted to an optical density (OD) using the Io signal from regions free of the catalyst particles. Chemical maps were obtained by fitting the OD stack to a set of reference spectra recorded from pure materials, as described in detail elsewhere [11].

2.3. Ptychography measurements, reconstruction, and analysis

Diffraction images (DI) at overlapping raster scanned positions were recorded using a CCD detector (Andor model DX434, 1024 × 1024 pixels). In order to convert the focused ~60 nm spot to a defocused spot size of either 1.25 or 3.0 μm diameter, the zone plate position was displaced along the X-ray axis. Dwell times of 1–3 s per diffraction image were used. Although DI of adequate quality can be achieved with sub-second dwell, longer dwells were used so as to have a better duty cycle, which is limited by the ~1 s/image transfer rate of the Andor camera. Sets of ptychographic DI were reconstructed using the PyPIE software package (developed by the CLS SM beamline team [26,28]), which is a CPU-based python program using the extended Python Iterative Engine (ePIE) algorithm. [34–38] Amplitude and phase images of both the object and the probe are generated by the PyPIE iterative reconstruction. The reconstructed amplitude and phase stacks were analyzed using aXis2000 [33,34] in a similar way as for STXM stacks. The amplitude images from the reconstruction are first aligned using Fourier cross-correlation. Following this, an area of the ptycho-amplitude-stack that does not have any catalyst particles is used

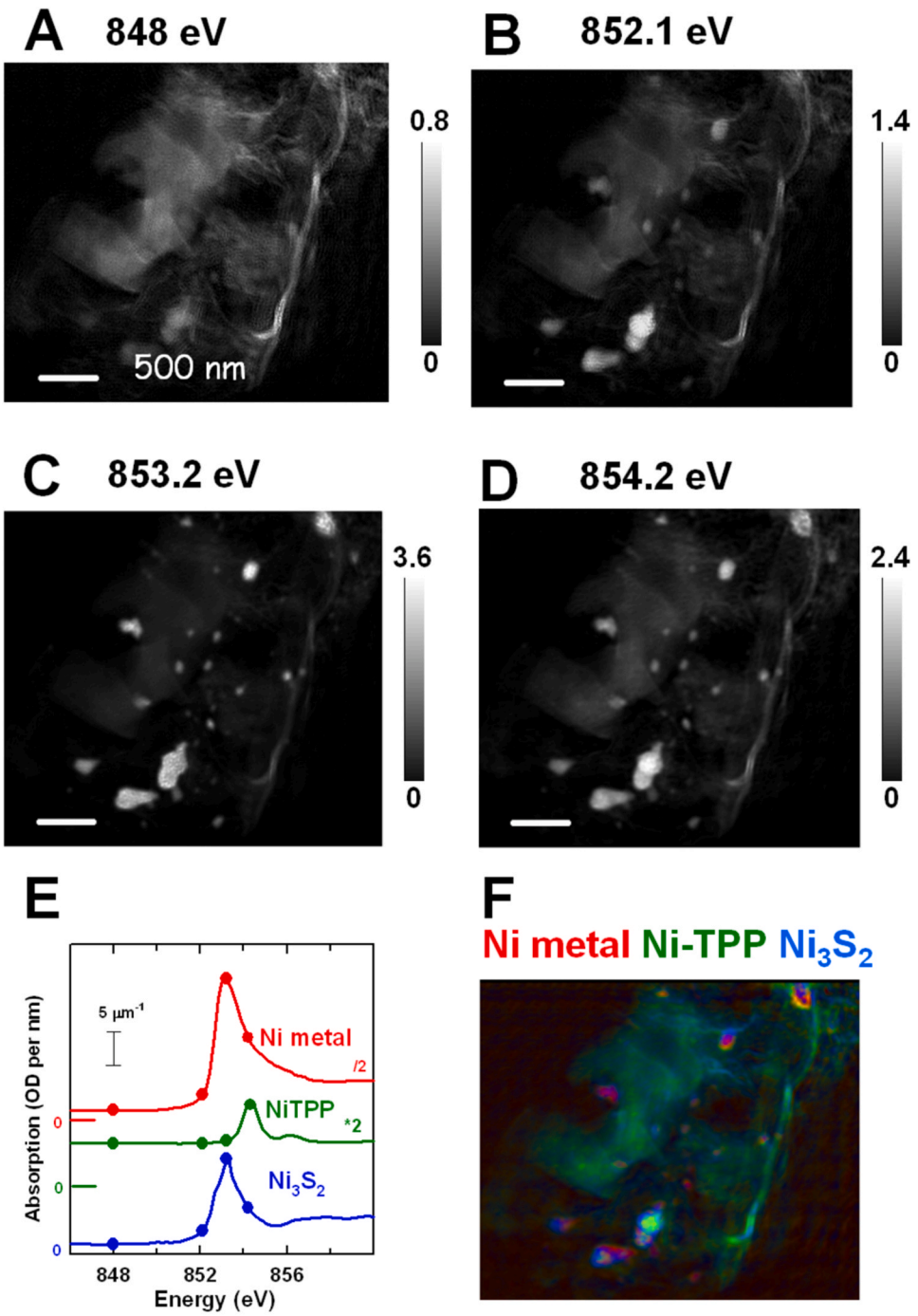

Fig. 2. Chemical mapping of a Ni-N-C-high catalyst aggregate by a 4-energy ptychography stack. Absorption images derived from reconstructed ptychography amplitude images at (a) 848 eV. (b) 852.1 eV (Ni metal). (c) 853.2 eV (Ni_3S_2) (d) 854.2 eV (Ni-TPP). All absorption images are plotted on the indicated grey scales. (e) Reference spectra of Ni metal, Ni-TPP and Ni_3S_2 on an optical density per unit thickness (OD1) scale with offsets, indicated by the color-coded zero of each curve, and scale factor, indicated by the 5 μm^{-1} vertical scale bar. The four energies sampled are indicated. (f) Rescaled color coded composite: Ni metal (red), Ni-TPP (green) and Ni_3S_2 (blue).

as an Io signal in the conversion of the ptycho-amplitude signal to the ptycho-absorption signal. For the phase images, Io normalization was not used [35] since the amplitude of a phase change signal should not be affected by the incident flux. In any case, there is no sharp spectral structure in the incident flux at the Ni L_3 edge. The Io signal does change by a factor of 2 over the energy range measured, which means that Io-normalized phase spectra would be tilted relative to that we present.

3. Results

3.1. Imaging: STXM versus ptychography

Fig. 1a shows a STXM transmission image at 853.9 eV of an agglomerated particle of the high-Ni loading Ni-N-C material. The image was measured using the fully focused spot from a 50 nm outer zone width zone plate. Fig. 1b shows the ptychography amplitude image, generated by reconstructing a ptychography data set measured at 853.9 eV using a 1.25 μm defocused spot size, and 90% overlap (4×4 μm, 32 ×32 samples, 1.7 s/DI). The much higher spatial resolution of the ptychography amplitude image is readily apparent. Some very small Ni nanoparticles (~20 nm) dispersed in the Ni-N-C sample are now observed, which could not be seen in the corresponding STXM image. Lines across sharp features indicate an apparent spatial resolution of 60 ± 10 nm for STXM and 20 ± 5 nm for ptychography. In a preliminary ptychography study of the Ni-N-C sample, a Fourier ring correlation (FRC) determined a half-pitch spatial resolution of 10 nm (see Fig. S19 of ref [9]), consistent with the 20 nm resolution estimated from line profiles across sharp features.

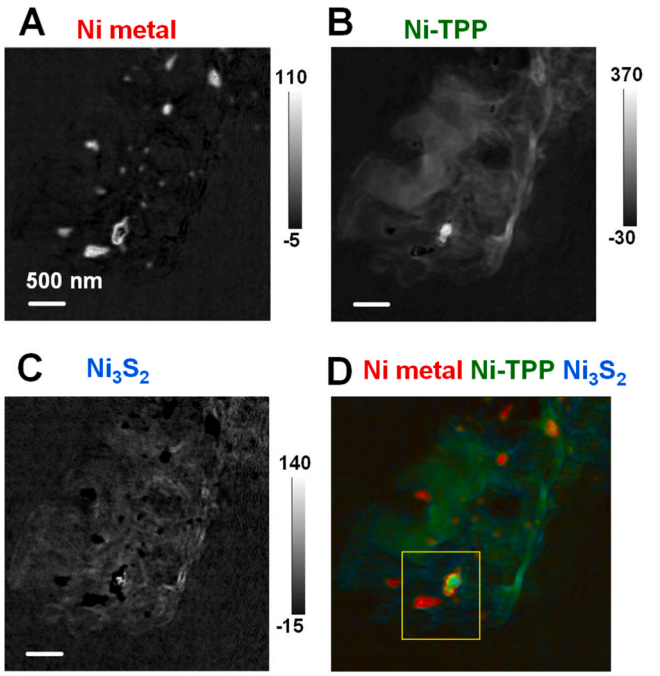

Fig. 3. Chemical mapping of Ni-N-C-high by a 34 energy Ni L_3 spectro-ptychography absorption stack. (a) component map of Ni metal. (b) component map of Ni single atom catalyst, as Ni-TPP. (c) component map of Ni_3S_2. The grey scale limits of each component map are thickness in nm. (d) rescaled colour-coded composite of the 3 component maps. (e) The reference spectra are plotted in Fig. 2e. The yellow box is the region expanded in Fig. 4. The ptychography stack was measured using a 2.0 μm spot to scan over $(4\ \mu m)^2$ area with $(10)^2$ points grid and 80% overlap with a dwell of 2.3 s.

3.2. Spectro-ptychography – amplitude

Fig. 2 presents the results of chemical mapping of the Ni-N-C-high catalyst aggregate by a 4-energy ptychography stack. These energies were chosen to best differentiate the Ni metal, Ni-TPP, and Ni_3S_2 species (see Fig. 2e). As found from the STXM study of the same particle [9], the Ni L_3 spectrum obtained from the carbonaceous region (areas that did not observably contain any particles) is well fit by the Ni L_3 spectrum of Ni-TPP. Meanwhile, the readily visible particles are best fit by a combination of Ni metal and Ni_3S_2, along with some Ni-TPP. Despite measuring only a few energies, the fit quality is excellent. The color-code chemical component maps derived from fitting the 4-E stack show that the nanoparticles mainly consist of Ni metal and Ni_3S_2, while the Ni-TPP signal is strongest in the matrix region. These results are qualitatively in good agreement with those derived from STXM measurements of the same sample [9].

Fig. 3 presents results from fitting a full, 34 energy spectro-ptychography absorption stack. The chemical component maps show the distribution of each Ni species. Ni metal and Ni_3S_2 mostly exist as components of the nanoparticles while the Ni-TPP signal is broadly dispersed in the matrix. This result is very similar to that derived from the 4-energy spectro-ptychography stack (Fig. 2) and that derived from the STXM stack reported in ref [9]. More importantly, since the reference spectra used in the analysis are on an absolute intensity scale – optical density per μm – the grey scale of each component map shown is quantitative, giving thickness in nm.

Fig. 4 is an expanded presentation of the results in Fig. 3, in the region indicated by the yellow box in Fig. 3d, which is a region with several of the larger particles. The particles are clearly a composite of different species, with an exterior dominated by Ni_3S_2 and an interior that is either Ni metal or a combination of Ni metal and Ni-TPP-like Ni-N-C single atom catalyst. A core-shell structure, with a sulfur-rich

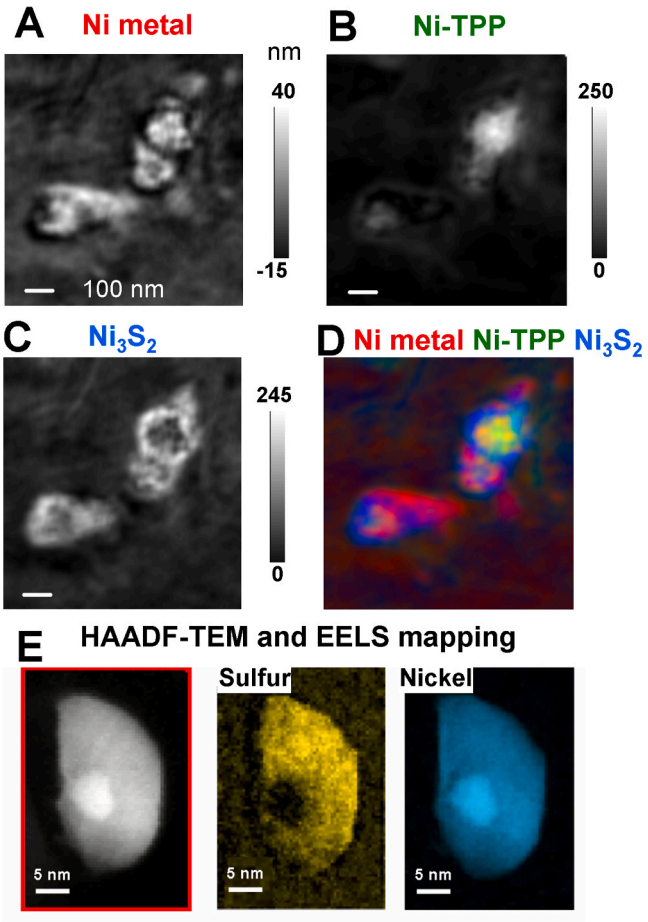

Fig. 4. Chemical mapping of particles in the Ni-N-C-high catalyst aggregate mapped by 4-energy ptychography. Quantitative maps (nm thickness) derived by fitting the 4E stack to the reference spectra (Fig. 2**e**). (a) Ni metal.(b) Ni-TPP. (c) Ni_3S_2 maps. (d) Rescaled color coded composite of the component maps after removal of pixels with large negative value, in order to better show the distribution of Ni components. Ni metal (red), Ni-TPP (green), Ni_3S_2 (blue). (e) TEM imaging and TEM-EELS sulfur and nickel mapping of an individual particle in the Ni-N-C-low sample. [9].

exterior and a Ni-rich core, had previously been observed by transmission electron microscopy combined with EELS mapping of some particles in the Ni-N-C-low sample, as shown in Fig. 4e (reproduced from Fig. 2 of [9]).

3.3. Spectro-ptychography – phase analysis

Ptychographic reconstruction provides an object scattering phase as well as the object scattering amplitude. A simultaneous analysis of the amplitude and phase signals, combined as an X-ray refractive index signal, would be preferable; an example of that approach has been reported by Farmand et al. [39] Alternatively, one can fit the phase stack to suitable phase reference signals. Although we have not measured phase spectra of the pure reference species by ptychography, we were able to derive these from the phase stack using regions of interest (ROI) defined by the component maps derived from the amplitude/absorption stack (Fig. 3).

Fig. 5 presents the phase spectra of the Ni metal, carbonaceous matrix region (Ni-TPP-like) and Ni_3S_4 extracted from the phase stack derived from the same ptychographic reconstruction of the 34 energy spectro-ptychography stack. The phase spectra have a typical 'derivative-like' shape [38,39]. The scattering phase shift signals from the denser, more crystalline Ni_3S_2 and Ni metal particles are much stronger

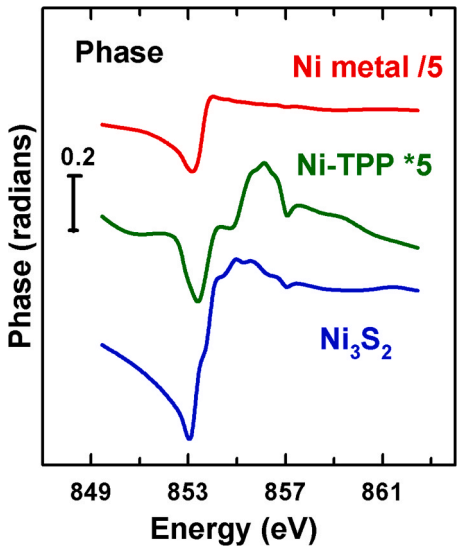

Fig. 5. Phase spectra of Ni metal, Ni-TPP and Ni_3S_2. The phase spectra are extracted from the phase stack for the Ni-N-C-high sample using regions of interest identified from the component maps derived from the analysis of the spectro-ptychography derived absorption stack (Fig. 3). The vertical scale bar, when combined with the indicated multiplicative factors, gives the scale of phase change for each phase-spectral component. The curves are offset for clarity.

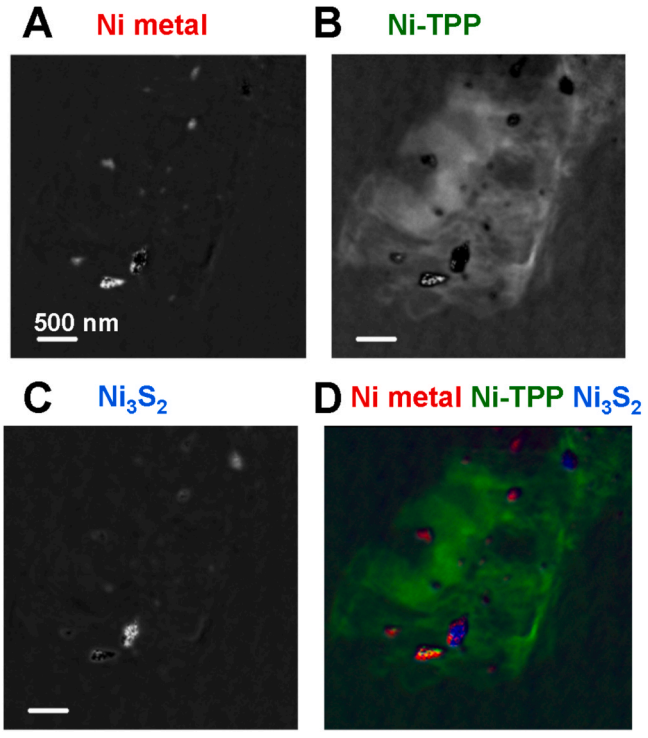

Fig. 6. Chemical mapping of a Ni-N-C-high aggregate by a 34 energy Ni L_3 spectro-ptychography phase stack. Component maps of (a) Ni metal, (b) Ni single atom catalyst, as Ni-TPP. (c) Ni_3S_2, derived by fitting the phase stack (from the same data set for which the absorption ptychography analysis is presented in Fig. 3) to the phase spectra presented in Fig. 5. (d) rescaled color coded composite of the 3 component maps.

than that from the TPP-like single atomic catalyst in the matrix. The first dip in the Ni metal and Ni_3S_2 phase signals occur at 853.1 eV (at the same energy as the absorption maximum in Ni metal but 0.3 eV below

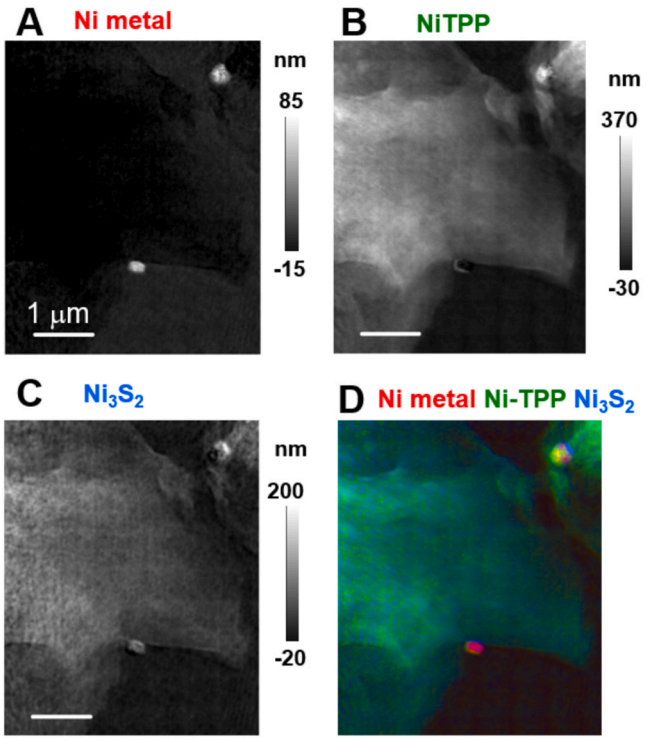

Fig. 7. Chemical mapping of Ni-N-C-low by a Ni L_3 spectro-ptychography absorption stack. Component maps of (a) Ni metal. (b) Ni single atom catalyst, as Ni-TPP. (c) Ni_3S_2, derived from a 34 energy Ni L_3 ptychography stack using 3 μm defocused spot to scan $(6)^2$ μm area with $(10)^2$ pixels and 1.7 s dwell time to achieve 80% overlap. The grey scale limits are thickness in nm. (d) Rescaled color coded composite of the 3 component maps. Reference spectra are plotted in Fig. 2e.

that of Ni_3S_2). The first dip in the phase signal of the carbonaceous matrix occurs at 853.3 eV, which is 0.9 eV below the maximum in the absorption spectrum of Ni-TPP. Chemical mapping based on these phase signals is presented in Fig. 6. In general, the component maps derived from the phase signals are in reasonable agreement with those derived from the ptychography amplitude signals. We note that the intensities in the ptychography phase-derived component maps are qualitative and cannot be related among the 3 species, since the connection between phase spectra and material thickness is not understood. This is in contrast to the quantitative thickness scales provided by analysis of the ptychography amplitude signals in the same way as STXM X-ray transmission signals.

3.4. *Ptychography of Ni-N-C-low*

In our previous study [9], the Ni-N-C low sample was shown to be a more efficient and selective CO_2 reduction catalyst than the Ni-N-C-high sample. The goal of the STXM study was to identify why. Fig. 7 presents chemical maps of the Ni-N-C-low sample derived from fits of the Ni metal, Ni-TPP, and Ni_3S_2 reference spectra (Fig. 2e) to the absorption images derived from amplitude images generated by reconstruction of a full spectro-ptychographic stack. Qualitatively, the spatial distributions of Ni components in the Ni-N-C-low sample are similar to that of the Ni-N-C-high sample shown in Fig. 3, but there are very few particles compared to the Ni-N-C high sample. In previous STXM studies for Ni-N-C-low samples, the observation of very few particles could have been attributed to the low spatial resolution of STXM such that that particles with size < 50 nm might widely exist but could not be detected. Here, the spectro-ptychographic results with a spatial resolution of ~20 nm, confirm there are very few nanoparticles with size > 20 nm in the Ni-N-C-low material. The spectro-ptychography results show that

the Ni-N-C-low material is quite homogeneous. This is favorable for the design of electrocatalysts and could be one of the reasons why Ni-N-C low shows better catalytic performance.

4. Discussion

Spectro-ptychography, measured using a defocused spot and a high degree of overlap, offers several specific advantages relative to conventional STXM. Radiation damage is frequently a significant limiting factor in high-resolution X-ray microscopy. [40–42] Recently, Mille et al. [24] presented a quantitative dose analysis for soft X-ray ptychography measured using a defocused probe and high overlap, conditions similar to the present study. That analysis showed that defocused spectro-ptychography delivers an appreciably lower dose and much lower dose density compared to STXM. For example, a STXM measurement of a single 4 μm* 4 μm image, using a 40 nm spot size and 2 ms dwell requires an exposure time of 20 s. In contrast, the corresponding ptychographic image measured using 500 ms dwell, 90% overlap and a 1.0 μm spot size (which has over 600 times lower dose density than the STXM conditions) would involve an exposure time of ~500 s. When the 600-fold lower dose density is factored in, the defocused, high-overlap ptychography delivers a dose equivalent to ~1 s of STXM. This ~20-fold lower radiation dose means there is correspondingly lower radiation damage. In addition, the longer dwell time means more X-ray-sample interaction and thus better statistical precision. Also, the long measurement time of each DI (relative to a single point in a full-focused STXM image) reduces the sensitivity of the results to artifacts from mechanical instabilities in the microscope, beamline and storage ring.

While the results presented here demonstrate the improved spatial resolution and statistical precision provided by ptychography, further improvements can be made. The existing CLS ambient STXM platform has relatively poor mechanical stability. A new STXM mechanism has been built and will be installed and commissioned by the end of 2023. The Andor CCD camera used for this study has a relatively slow image transfer speed. A new generation of direct X-ray sensitive sCMOS cameras for the soft X-ray region are now available which have much faster data transfer rates (for example, current generation sCMOS devices can transfer a 1 Mpixel image in 40 ms). Such sCMOS cameras have been used for low energy spectro-ptychography studies [24,25] including a very recent spectro-ptychography study of a Cu carbon dioxide reduction (CO2R) catalyst under in-situ flow electrochemical control conditions [43].

This spectro-ptychography study has provided chemical and morphological information with a significantly superior spatial resolution to that provided by our earlier STXM study. [9] The spectro-ptychography analysis of the few-particle area (Fig. 4), although still at a much lower spatial resolution than the TEM imaging and EELS mapping reported earlier [9], is consistent with the previous conclusion that core-shell particles, with Ni metal surrounded by Ni_3S_2, tend to form with the synthesis conditions for Ni-N-C-high. Lowering the Ni content and reducing the amount of Ni metal-rich nanoparticles increases the homogeneity which was previously shown [9] to improve the Faradaic efficiency for the reduction of CO_2 to CO.

Declaration of Competing Interest

The authors declare that they have no known competing financial interests or personal relationships that could have appeared to influence the work reported in this paper.

Data availability

Data will be made available on request.

Acknowledgments

Research is supported by the Natural Sciences and Engineering Research Council (NSERC) Discovery grant and the National Research Council of Canada's Materials for Clean Fuels Challenge program. Measurements were made using the ambient STXM on beamline 10ID1 at the Canadian Light Source (CLS), which is supported by CFI, NSERC, CIHR, NRC, and the University of Saskatchewan. Electron microscopy was performed at the Canadian Centre for Electron Microscopy at McMaster University.

References

[1] A.S. Varela, W. Ju, A. Bagger, P. Franco, J. Rossmeisl, P. Strasser, Electrochemical reduction of CO_2 on metal-nitrogen-doped carbon catalysts, ACS Catal. 9 (2019) 7270–7284.
[2] A.A. Gewirth, J.A. Varnell, A.M. DiAscro, Nonprecious metal catalysts for oxygen reduction in heterogeneous aqueous systems. Chem. Rev. 118 (2018) 2313–2339.
[3] J. Zhang, Z. Xia, L. Dai, Carbon-based electrocatalysts for advanced energy conversion and storage. Sci. Adv. 1 (2015), e1500564.
[4] Z. Chen, D. Higgins, A. Yu, L. Zhang, J. Zhang, A review on non-precious metal electrocatalysts for PEM fuel cells. Energy Environ. Sci. 4 (2011) 3167–3192.
[5] D.M. Koshy, S. Chen, D.U. Lee, M.B. Stevens, A.M. Abdellah, S.M. Dull, G. Chen, D. Nordlund, A. Gallo, C. Hahn, D.C. Higgins, Z. Bao, T.F. Jaramillo, Understanding the origin of highly selective CO_2 electroreduction to CO on Ni, N-doped carbon catalysts, Angew. Chem. 132 (2020) 4072–4079.
[6] D.M. Koshy, A.T. Landers, D.A. Cullen, A.V. Ievlev, H.M. Meyer III, C. Hahn, Z. Bao, T.F. Jaramillo, Direct characterization of atomically dispersed catalysts: nitrogen coordinated ni sites in carbon-based materials for CO electroreduction, Adv. Energy Mater. 10 (2020), 2001836.
[7] Y. Cheng, S. Zhao, H. Li, S. He, J.-P. Veder, B. Johannessen, J. Xiao, S. Lu, J. Pan, M.F. Chisholm, S.-Z. Yang, C. Liu, J.G. Chen, S.P. Jiang, Unsaturated edge-anchored Ni single atoms on porous microwave exfoliated graphene oxide for electrochemical CO_2, Appl. Catal. B: Environ. 243 (2019) 294–303.
[8] Y. Chen, S. Ji, S. Zhao, W. Chen, J. Dong, W.-C. Cheong, R. Shen, X. Wen, L. Zheng, A.I. Rykov, S. Cai, H. Tang, Z. Zhuang, C. Chen, Q. Peng, D. Wang, Y. Li, Enhanced oxygen reduction with single-atomic-site iron catalysts for a zinc-air battery and hydrogen-air fuel cell. Nat. Commun. 9 (2018) 1–12.
[9] C. Zhang, L. Shahcheraghi, F. Ismail, H. Eraky, H. Yuan, A.P. Hitchcock, D. Higgins, Ni-N-C electrocatalysts for CO_2 reduction studied by scanning X-ray transmission X-ray microscopy, ACS Catal. 12 (2022) 8746–8760.
[10] H. Ade, A.P. Hitchcock, NEXAFS microscopy and resonant scattering: Composition and orientation probed in real and reciprocal space, Polymer 49 (2008) 643–675.
[11] Hitchcock, A.P. Soft X-Ray Imaging and Spectromicroscopy. In Handbook of Nanoscopy Vol. 2, Tendeloo, G. Van, Dyck, V.D., Pennycook, S.J., Eds.; Wiley-VCH Verlag GmbH & Co. KGaA: Weinheim, Germany, 2012, 745–791.
[12] S. Zhao, Y. Cheng, J.-P. Veder, B. Johannessen, M. Saunders, L. Zhang, C. Liu, M. F. Chisholm, R. De Marco, J. Liu, S.-Z. Yang, S.P. Jiang, One-pot pyrolysis method to fabricate carbon nanotube supported Ni single-atom catalysts with ultrahigh loading, ACS Appl. Energy Mater. 1 (2018) 5286–5297.
[13] H.T. Chung, D.A. Cullen, D. Higgins, B.T. Sneed, E.F. Holby, K.L. More, P. Zelenay, Direct atomic-level insight into the active sites of a high-performance PGM-Free ORR catalyst, Science 357 (2017) 479–484.
[14] J. Timoshenko, B. Roldan Cuenya, In situ/operando electrocatalyst characterization by x-ray absorption spectroscopy, Chem. Rev. 121 (2021) 882–896.
[15] H.-T. Lien, S.-T. Chang, P.-T. Chen, D.P. Wong, Y.-C. Chang, Y.-R. Lu, C.-L. Dong, C.-H. Wang, K.-H. Chen, L.-C. Chen, Probing the active site in single-atom oxygen reduction catalysts via operando X-ray and electrochemical spectroscopy, Nat. Commun. 11 (2020) 4233.
[16] F. Pfeiffer, X-ray ptychography, Nat. Photonics 12 (2018) 9–17.
[17] Rodenburg, J.; Maiden, A. Ptychography. *Springer Handbook of Microscopy*; Springer International Publishing: Switzerland, 16 (2019) 819−904.
[18] D.A. Shapiro, Y.-S. Yu, T. Tyliszczak, J. Cabana, R. Celestre, W. Chao, K. Kaznatcheev, K. David, F. Maia, S. Marchesini, Y. Meng, T. Warwick, L. Yang, H. Padmore, Chemical composition mapping with nano-metre resolution by soft X-ray microscopy, Nat. Photonics 8 (2014) 765–769.
[19] A.P. Hitchcock, Soft X-ray spectromicroscopy and ptychography, J. Electron Spectrosc. Relat. Phenom. 200 (2015) 49–63.
[20] X.H. Zhu, A.P. Hitchcock, D.A. Bazylinski, P. Denes, J. Joseph, U. Lins, S. Marchesini, H.-W. Shiu, T. Tyliszczak, D.A. Shapiro, Measuring spectroscopy and magnetism of extracted and intracellular magnetosomes using soft X-ray ptychography, Proc. Natl. Acad. Sci. 113 (2016) E8219–E8227.
[21] J. Wu, X. Zhu, M.M. West, T. Tyliszczak, H.-W. Shiu, D. Shapiro, V. Berejnov, D. Susac, J. Stumper, A.P. Hitchcock, High resolution imaging of polymer electrolyte membrane fuel cell cathode layers by soft X-ray spectro-ptychography, J. Phys. Chem. C. 122 (2018) 11709–11719.
[22] D.A. Shapiro, S. Babin, R.S. Celestre, W. Chao, R.P. Conley, P. Denes, B. Enders, P. Enfedaque, S. James, J.M. Joseph, H. Krishnan, S. Marchesini, K. Muriki, K. Nowrouzi, S.R. Oh, H. Padmore, T. Warwick, L. Yang, V.V. Yashchuk, Y.-S. Yu, J. Zhao, An ultrahigh-resolution soft x-ray microscope for quantitative analysis of chemically heterogeneous nanomaterials, Sci. Adv. 6 (2020) eabc4904.

[23] H. Yuan, H. Yuan, T. Casagrande, D. Shapiro, Y.-S. Yu, B. Enders, J.R.I. Lee, A. van Buuren, M.M. Biener, S.A. Gammon, T.F. Baumann, A.P. Hitchcock, *4*D imaging of ZnO-coated nanoporous Al_2O_3 aerogels by chemically-sensitive ptychographic tomography: implications for designer catalysts, ACS Appl. Nanomater. 4 (2021) 621–632.
[24] N. Mille, H. Yuan, J. Vijayakumar, S. Stanescu, S. Swaraj, K. Desjardins, V. Favre-Nicolin, R. Belkhou, A.P. Hitchcock, Ptychography at the carbon K-edge, Commun. Mater. 3 (2022) 8.
[25] J. Vijayakumar, N. Mille, H. Yuan, S. Stenescu, S. Swaraj, K. Desjardins, F. Orsini, V. Favre-Nicolin, E. Najafi, A.P. Hitchcock, R. Belkhou, Soft X-ray spectro-ptychography of boron nitride nanobamboos, carbon nanotubes and permalloy nanorods, J. Synchrotron Radiat. 30 (2023) 746–757.
[26] T. Sun, G. Sun, F. Yu, Y. Mao, R. Tai, X. Zhang, G. Shao, Z. Wang, J. Wang, J. Zhou, "Soft X-Ray ptychography chemical imaging of degradation in a composite surface-reconstructed Li-rich cathode, ACS Nano 15 (2021) 1475–1485.
[27] X. Xia, J. Wang, Y. Hu, J. Liu, A.I. Darma, L. Jin, H. Han, C. He, J. Yang, Molecular insights into roles of dissolved organic matter in Cr(III) immobilization by coprecipitation with Fe(III) probed by STXM-ptychography and XANES spectroscopy, Environ. Sci. Technol. 56 (2022) 2432–2442.
[28] T. Sun, S. Zuo, B. He, X. Yuan, G. Li, J. Zhou, A. Abate, J. Wang, Ionic liquid functionalized tin halide perovskite investigated by STXM and spectro-ptychography, J. Electron Spectrosc. Rel. Phenomena 265 (2023), 147330.
[29] L. Shahcheraghi, C. Zhang, H.-J. Lee, M. Cusack-Striepe, F. Ismail, A. Abdellah, D. C. Higgins, Identifying activity and selectivity trends for the electrosynthesis of hydrogen peroxide via oxygen reduction on nickel–nitrogen–carbon catalysts, J. Phys. Chem. C. 125 (2021) 15830–15840.
[30] K.V. Kaznatcheev, C. Karunakaran, U.D. Lanke, S.G. Urquhart, M. Obst, A. P. Hitchcock, Soft X-ray spectromicroscopy beamline at the CLS: Commissioning results, Nucl. Instrum. Methods Phys. Res. Sect. A: Accel. Spectrom. Detect. Assoc. Equip. 582 (2007) 96–99.
[31] C. Jacobsen, S. Wirick, G. Flynn, C. Zimba, Soft x-ray spectroscopy from image sequences with sub-100 nm spatial resolution, J. Microsc. 197 (2000) 173–184.
[32] A.P. Hitchcock, C.E. Brion, Neon K-shell excitation studied by electron energy-loss spectroscopy, J. Phys. B: At. Mol. Phys. 13 (1980) 3269–3273.
[33] Hitchcock, A.P. aXis2000 Is written in Interactive Data Language (IDL). It is available free for non-commercial use from http//unicorn.mcmaster.ca/aXis2000.html (last accessed 23 April 2023.
[34] A.P. Hitchcock, Analysis of X-ray Images and Spectra (aXis2000) – a toolkit for X-ray spectromicroscopists, J. Electron Spectrosc. Rel. Phenomena 266 (2023), 147360.
[35] S.G. Urquhart, X-ray spectro-ptychography, ACS Omega 7 (2022) 11521–11529.
[36] F. Zhang, I. Peterson, J. Vila-Comamala, A. Diaz, F. Berenguer, R. Bean, B. Chen, A. Menzel, I.K. Robinson, J.M. Rodenburg, Translation position determination in ptychographic coherent diffraction imaging, Opt. Express 21 (2013) 13592–13606.
[37] J.R. Fienup, Reconstruction of an object from the modulus of its fourier transform, Opt. Lett. 3 (1978) 27–29.
[38] J.M. Rodenburg, H.M.L. Faulkner, A phase retrieval algorithm for shifting illumination, Appl. Phys. Lett. 85 (2004) 4795–4797.
[39] M. Farmand, R. Celestre, P. Denes, A.L.D. Kilcoyne, S. Marchesini, H. Padmore, T. Tyliszczak, T. Warwick, X. Shi, J. Lee, Y.-S. Yu, J. Cabana, J. Joseph, H. Krishnan, T. Perciano, F.R.N.C. Maia, D.A. Shapiro, Near-edge X-ray refraction fine structure microscopy, Appl. Phys. Lett. 110 (2017), 063101.
[40] J. Wang, G.A. Botton, M.M. West, A.P. Hitchcock, Quantitative evaluation of radiation damage to polyethylene terephthalate by soft X-rays and high energy electrons, J. Phys. Chem. B 113 (2009) 1869–1876.
[41] J. Wang, C. Morin, L. Li, A.P. Hitchcock, X. Zhang, T. Araki, A. Doran, A. Scholl, Radiation damage in soft x-ray microscopy, J. Electron Spectrosc. Rel. Phenom. 170 (2009) 25–36.
[42] I. Martens, L.G.A. Melo, D. Wilkinson, D. Bizzotto, A.P. Hitchcock, Characterization of X-ray damage to perfluorosulfonic acid using correlative microscopy, J. Phys. Chem. C. 123 (2019) 16023–16033.
[43] C. Zhang, H. Eraky, N. Mille, S. Stanescu, S. Swaraj, R. Belkhou, D. Higgins, A. P. Hitchcock, Copper CO_2-reduction electrocatalysts studied by in-situ Soft X-ray spectro-ptychography, Chem. Catal. (2023) (in review).